

High-frequency self-induced oscillations in a silicon nanocavity

Nicolas Cazier, Xavier Checoury,* Laurent-Daniel Haret and Philippe Boucaud

*Institut d'Electronique Fondamentale. Bâtiment 220, Univ. Paris Sud
CNRS UMR 8622 F-91405 Orsay France*

[*xavier.checoury@ief.u-psud.fr](mailto:xavier.checoury@ief.u-psud.fr)

Abstract: We show that self-induced oscillations at frequencies above GHz and with a high spectral purity can be obtained in a silicon photonic crystal nanocavity under optical pumping. This self-pulsing results from the interplay between the nonlinear response of the cavity and the photon cavity lifetime. We provide a model to analyze the mechanisms governing the onset of self-pulsing, the amplitudes of both fundamental and harmonic oscillations and their dependences versus input power and oscillation frequency. Theoretically, oscillations at frequencies higher than 50 GHz could be achieved in this system.

© 2013 Optical Society of America

OCIS codes: (230.5298) Photonic crystals; (190.4390) Nonlinear optics, integrated optics; (230.4910) Oscillators; (140.3948) Microcavity devices.

References and links

1. Y. Akahane, T. Asano, B. S. Song, and S. Noda, "High-Q photonic nanocavity in a two-dimensional photonic crystal," *Nature (London)* **425**, 944–947 (2003).
2. B. S. Song, S. Noda, T. Asano, and Y. Akahane, "Ultra-high-Q photonic double-heterostructure nanocavity," *Nat. Mater.* **4**, 207–210 (2005).
3. Y. Takahashi, Y. Tanaka, H. Hagino, T. Sugiya, Y. Sato, T. Asano, and S. Noda, "Design and demonstration of high-Q photonic heterostructure nanocavities suitable for integration," *Opt. Express* **17**, 18093–18102 (2009).
4. M. Soljačić and J. D. Joannopoulos, "Enhancement of nonlinear effects using photonic crystals," *Nat. Mater.* **3**, 211–219 (2004).
5. P. Barclay, K. Srinivasan, and O. Painter, "Nonlinear response of silicon photonic crystal microresonators excited via an integrated waveguide and fiber taper," *Opt. Express* **13**, 801–820 (2005).
6. C. Monat, B. Corcoran, M. Ebnali-Heidari, C. Grillet, B. J. Eggleton, T. P. White, L. O'Faolain, and T. F. Krauss, "Slow light enhancement of nonlinear effects in silicon engineered photonic crystal waveguides," *Opt. Express* **17**, 2944–2953 (2009).
7. T. Tanabe, M. Notomi, S. Mitsugi, A. Shinya, and E. Kuramochi, "Fast bistable all-optical switch and memory on a silicon photonic crystal on-chip," *Opt. Lett.* **30**, 2575–2577 (2005).
8. X. Checoury, Z. Han, and P. Boucaud, "Stimulated Raman scattering in silicon photonic crystal waveguides under continuous excitation," *Phys. Rev. B* **82**, 041308(R) (2010).
9. J. F. McMillan, M. B. Yu, D. L. Kwong, and C. W. Wong, "Observation of four-wave mixing in slow-light silicon photonic crystal waveguides," *Opt. Express* **18**, 15484–15497 (2010).
10. J. Capmany and D. Novak, "Microwave photonics combines two worlds," *Nat. Photonics* **1**, 319–330 (2007).
11. S. Malaguti, G. Bellanca, A. de Rossi, S. Combrì, and S. Trillo, "Self-pulsing driven by two-photon absorption in semiconductor nanocavities," *Phys. Rev. A* **83**, 051802 (2011).
12. K. Ikeda and O. Akimoto, "Instability leading to periodic and chaotic self-pulsations in a bistable optical cavity," *Phys. Rev. Lett.* **48**, 617–620 (1982).
13. S. Chen, L. Zhang, Y. Fei, and T. Cao, "Bistability and self-pulsation phenomena in silicon microring resonators based on nonlinear optical effects," *Opt. Express* **20**, 7454–7468 (2012).
14. T. J. Johnson, M. Borselli, and O. Painter, "Self-induced optical modulation of the transmission through a high-Q silicon microdisk resonator," *Opt. Express* **14**, 817–831 (2006).

15. M. Brunstein, A. M. Yacomotti, I. Sagnes, F. Raineri, L. Bigot, and A. Levenson, "Excitability and self-pulsing in a photonic crystal nanocavity," *Phys. Rev. A* **85**, 031803– (2012).
16. M. Soltani, S. Yegnanarayanan, Q. Li, A. A. Eftekhari, and A. Adibi, "Self-sustained gigahertz electronic oscillations in ultrahigh-Q photonic microresonators," *Phys. Rev. A* **85**, 053819 (2012).
17. E. Kuramochi, M. Notomi, S. Mitsugi, A. Shinya, T. Tanabe, and T. Watanabe, "Ultrahigh-Q photonic crystal nanocavities realized by the local width modulation of a line defect," *Appl. Phys. Lett.* **88**, 041112 (2006).
18. Z. Han, X. Checoury, D. Néel, S. David, M. El Kurdi, and P. Boucaud, "Optimized design for 2×10^6 ultra-high Q silicon photonic crystal cavities," *Opt. Commun.* **283**, 4387–4391 (2010).
19. Z. Han, X. Checoury, L.-D. Haret, and P. Boucaud, "High quality factor in a two-dimensional photonic crystal cavity on silicon-on-insulator," *Opt. Lett.* **36**, 1749–1751 (2011).
20. T. Uesugi, B. S. Song, T. Asano, and S. Noda, "Investigation of optical nonlinearities in an ultra-high-Q Si nanocavity in a two-dimensional photonic crystal slab," *Opt. Express* **14**, 377–386 (2006).
21. Q. Lin, O. J. Painter, and G. P. Agrawal, "Nonlinear optical phenomena in silicon waveguides: modeling and applications," *Opt. Express* **15**, 16604–16644 (2007).
22. T. Tanabe, H. Sumikura, H. Taniyama, A. Shinya, and M. Notomi, "All-silicon sub-Gb/s telecom detector with low dark current and high quantum efficiency on chip," *Appl. Phys. Lett.* **96**, 101103 (2010).
23. L.-D. Haret, X. Checoury, Z. Han, P. Boucaud, S. Combrié, and A. D. Rossi, "All-silicon photonic crystal photodetector on silicon-on-insulator at telecom wavelength," *Opt. Express* **18**, 23965–23972 (2010).
24. A. Armaroli, S. Malaguti, G. Bellanca, S. Trillo, A. de Rossi, and S. Combrié, "Oscillatory dynamics in nanocavities with noninstantaneous Kerr response," *Phys. Rev. A* **84**, 053816 (2011).
25. T. J. Johnson and O. Painter, "Passive modification of free carrier lifetime in high-Q silicon-on-insulator optics," 2009 Conference On Lasers and Electro-optics and Quantum Electronics and Laser Science Conference (CLEO/QELS 2009), **1-5**, 72–73 (2009).
26. P. Grinberg, K. Bencheikh, M. Brunstein, A. M. Yacomotti, Y. Dumeige, I. Sagnes, F. Raineri, L. Bigot, and J. A. Levenson, "Nanocavity linewidth narrowing and group delay enhancement by slow light propagation and nonlinear effects," *Phys. Rev. Lett.* **109**, 113903 (2012).
27. S. Kaka, M. R. Pufall, W. H. Rippard, T. J. Silva, S. E. Russek, and J. A. Katine, "Mutual phase-locking of microwave spin torque nano-oscillators," *Nature (London)* **437**, 389–392 (2005).
28. A. C. Turner-Foster, M. A. Foster, J. S. Levy, C. B. Poitras, R. Salem, A. L. Gaeta, and M. Lipson, "Ultrashort free-carrier lifetime in low-loss silicon nanowaveguides," *Opt. Express* **18**, 3582–3591 (2010).
29. If we consider that the transmitted signal is detected by a photodetector, the RF power is proportional to the square of the electric intensity generated by the photodetector, i.e. to the square of the optical intensity.
30. M. Dinu, F. Quochi, and H. Garcia, "Third-order nonlinearities in silicon at telecom wavelengths," *Appl. Phys. Lett.* **82**, 2954–2956 (2003).
31. H. H. Li, "Refractive index of silicon and germanium and its wavelength and temperature derivatives," *J. Phys. and Chem. Ref. Data* **9**, 98 (1980).
32. T. Tanabe, H. Taniyama, and M. Notomi, "Carrier diffusion and recombination in photonic crystal nanocavity optical switches," *J. Lightwave Tech.* **26**, 1396–1403 (2008).

Cavities made in photonic crystals are characterized by their very small modal volume V of the order of $(\lambda/n)^3$ and their high quality factor Q [1–3]. Because the strength of light-matter interactions in the cavity depends on the ratio Q/V , the field of nonlinear photonic crystals has rapidly emerged for photonic applications and all-optical signal processing [4]. Devices with small footprint and very low switching energies are expected thanks to the enhanced non-linear response. Several nonlinear phenomena like two-photon absorption (TPA), third-harmonic generation, four-wave mixing, optical bistability, stimulated Raman scattering have been consequently demonstrated in photonic crystals by different groups [5–9]. One very attractive feature of nonlinear dynamics is its application to microwave photonics. Microwave photonics aims to provide functions that are complex to obtain in the radio-frequency domain [10]. In particular, optical generation and distribution of microwave signals in a very compact system are key techniques. It has been theoretically shown that self-pulsation at high frequencies (up to 100 GHz) could be obtained in resonant systems like photonic crystal cavities in the presence of strong nonlinearities [11]. Self-pulsing is an intrinsic property of nonlinear systems characterized by delay-differential dynamics [12] and results from the balance between the nonlinear response and the photon cavity lifetime. One key feature of optical microcavities is that the photon lifetime can be in the same range as the carrier lifetime. In this case, self-pulsing can be triggered by the interaction between free-carrier dispersion and TPA [11, 13]. TPA creates a local carrier

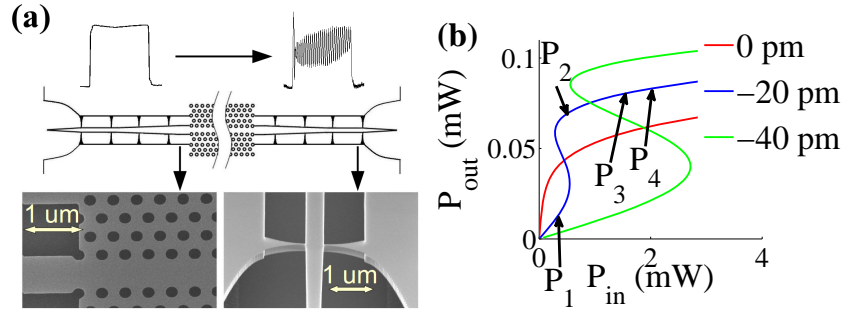


Fig. 1. (a) (top): schematic view of the photonic crystal with the suspended access waveguides and nanotethers. The input light pulse intensity and the oscillating output are also drawn schematically. Bottom: scanning electron microscope view of the entrance of the photonic crystal waveguide (left) and view of an access waveguide (right). (b) Simulated steady-state output power of the cavity as a function of the input power for different detunings of the pump. For the curve at a detuning of -20 pm, the zone of bistability is between $P_1 = 0.284$ mW and $P_2 = 0.549$ mW. Self-pulsation can be observed for input powers larger than $P_3 = 1.5$ mW, above the zone of bistability. The measurement reported in Fig. 3 (b) was performed for an input power $P_4 = 2$ mW.

plasma that shifts the cavity resonance because of the photo-induced refractive index variation. The achievement of self-sustained oscillations requires a positive feedback mechanism. The latter is provided by the dynamical tuning of the cavity resonance as a function of the carrier density that modulates the stored energy in the cavity. This self-pulsing effect can be obtained at GHz frequencies and differs therefore significantly from the one created by the competition of thermal and free-carrier effects, which is limited to MHz frequencies [14, 15]. Here, we experimentally show that non-attenuated self-induced spontaneous oscillations can occur in silicon photonic crystal (PhC) nanocavities at frequencies near 3 GHz, a value much higher than those that have been recently demonstrated in silicon microring resonators [16]. Despite the fact that the oscillations originate from nonlinear effects, the observed oscillations in silicon PhC cavities are almost perfectly sinusoidal and this counterintuitive property is precisely explained by the analytical model presented in this letter.

The membrane photonic crystal nanocavity studied here is a modulated-width waveguide cavity following the design in [17]. Light was injected in the cavity and collected with lensed fibers through ridge-type access waveguides suspended by nano-tethers as in [18] (see Fig. 1(a)). A direct coupling between cavity and access waveguides is implemented as illustrated in [19]. The measured coupling loss from the lensed fiber to each access waveguide is 8 dB and the input and output powers given afterward are those at the entrance and exit of the photonic crystal. A continuous tunable external cavity laser is modulated by a Mach-Zehnder modulator to generate 10-ns duration pulses with a repetition rate of 100 kHz in order to minimize thermal effects. A 6-GHz bandwidth InGaAs photodiode is used to detect the output signal. In the present experiment, the peak resonance of the studied cavity is at 1585.638 nm, its quality factor Q is around 130000 and the transmission at the resonance is $T_{max} = 41\%$ between the entrance and exit of the photonic crystal. Figure 1(b) shows the calculated output power as a function of the input power for different detunings between the laser and the cavity resonance. We can clearly observe the cavity nonlinear behavior as the power is increased. Bistability is obtained when the pump has a negative detuning as compared to the resonance wavelength, i.e. when the laser wavelength is shorter than the cavity resonance wavelength. As explained in [11] and in appendix 2, self-pulsing can be expected for operating points on the high-energy

branch that characterizes the output power. The occurrence of spontaneous oscillations is very dependent on the carrier recombination time and on a fine tuning of different parameters that can be chosen based on the modeling of the silicon nanocavity.

The equations describing the temporal behavior of the cavity are [11, 20, 21]:

$$\frac{dA}{dt} = -\frac{A}{2\tau} + i\Delta\omega A - \gamma^{FCA} \frac{N}{V_{eff}} A - \frac{\gamma^{TPA} |A|^2 A}{2\hbar\omega} + \sqrt{\frac{P_{in}}{\tau_{in}}} \quad (1)$$

$$\frac{dN}{dt} = -\frac{N}{\tau_{fc}} + \frac{1}{2} \gamma^{TPA} \frac{|A|^4}{(\hbar\omega)^2} \quad (2)$$

where A is the complex amplitude of the electrical field of the confined mode in the cavity (with $E = |A|^2$ the mode energy) and N is the number of free-carriers. The first term on the right-hand side of Eq. (1), $-A/(2\tau)$ represents the damping of the electrical field due to intrinsic linear losses, $\tau = Q/\omega_0$, being the photon lifetime in the cavity. This field decay is compensated by the continuous injection of light into the cavity that is taken into account by the last term $\sqrt{P_{in}/\tau_{in}}$, $\tau_{in} = 2\tau/\sqrt{T_{max}}$ being the photon injection time and T_{max} the transmission maximum at low input power. The interplay between the second term, $i\Delta\omega A$, and the third term, $-\gamma^{FCA} \frac{N}{V_{eff}} A$, is mainly responsible for the oscillations of the cavity: $\Delta\omega = \omega - \omega_0$ represents the detuning between the input laser frequency $\omega/(2\pi)$ and the cavity resonance frequency $\omega_0/(2\pi)$. $-\gamma^{FCA} \frac{N}{V_{eff}} A$, where γ^{FCA} is a complex number, represents the effect of free-carrier induced absorption and dispersion, and V_{eff} is the cavity effective volume over which the photo-generated free-carriers spread (see appendix 1 Free-carrier dispersion, absorption and generation). Here, we calculated $\gamma^{FCA} = 5.83 \times 10^{-14} + 1.7 \times 10^{-12}i \text{ m}^3 \text{ s}^{-1}$ using three-dimensional finite difference in time domain (3D-FDTD) simulation.

The fourth term in Eq. (1) represents the effect of two-photon absorption. For the power considered here, this term has a negligible effect on the cavity field decay but its counterpart in Eq. (2), $\frac{1}{2} \gamma^{TPA} \frac{|A|^4}{(\hbar\omega)^2}$, is crucial. Indeed, it represents the unique source term in the equation for free-carriers, $-1/\tau_{fc}$ being the effective decay rate of free carriers. From 3D-FDTD, we deduced $\gamma^{TPA} = 1.63 \times 10^4 \text{ s}^{-1}$ for the PhC cavity.

For the input power we used experimentally ($P = 2 \text{ mW}$), the linear absorption that exists in structured silicon [22, 23] is negligible as compared to TPA. For the same reason, we did not take into account the dispersion created by Kerr effect since it is negligible when compared to the dispersion created by free-carriers [24].

Classically, this system of differential equations can be solved by first looking for steady state solutions and then by linearizing for small variations around these steady-state solutions (see Refs. [11, 13, 16] and appendix 2 Solving the equations: steady state and small perturbations). Steady-state solutions of the different variables of the system can be expressed as a function of the energy $E = |A|^2$ that appears as a root of a five-degree polynomial. As mentioned before, self-pulsing only happens for a high value of E , i.e. on the upper energy-branch and beyond the bistability zone. The eigenvalues of the matrix associated to this linearized system around the steady-state solutions characterize the cavity dynamics. Self-induced oscillations occur when the system is characterized by a Hopf bifurcation which happens when a pair of conjugate eigenvalues $\alpha_r \pm i\Omega$ goes from the left half complex plane to the right one as a parameter of the system is varied, i.e. when the real part of these eigenvalues becomes positive. The oscillations are non-attenuated for $\alpha_r > 0$, corresponding to an equivalent gain and their period is $2\pi/\Omega$.

The set of parameters where self-pulsing occurs is illustrated in Fig. 2. Figure 2(a) shows that, for a cavity with $Q=130000$, non-attenuated oscillations can only be obtained for a free-carrier lifetime smaller than 0.4 ns and a cavity effective volume smaller than $5.5 \mu\text{m}^3$. Figure 2(b) shows the dependence of the oscillation period for a free-carrier lifetime of 0.2 ns and an

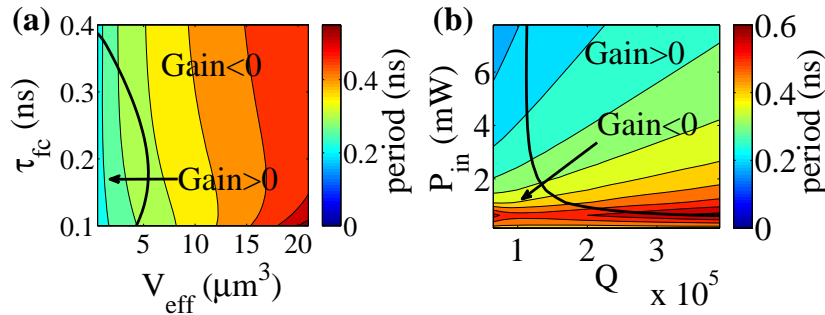


Fig. 2. (a) Period of the oscillations as a function of the cavity effective volume V_{eff} and the free-carrier lifetime, for a cavity with a quality factor $Q=130000$, a detuning of -20 pm and an input power $P_4 = 2$ mW. The oscillations are non-attenuated in the zone of positive gain (inside the region defined by the black thick line). (b) Period of the oscillations as a function of the quality factor and input power for a free-carrier lifetime of 0.2 ns and an effective volume $V_{eff} = 5.25 \mu m^3$.

effective volume $V_{eff} = 5.25 \mu m^3$ and indicates that, in this case, self-sustained oscillations can only be obtained for a quality factor higher than 110000. In the latter case, when we plot the cavity energy vs. the number of free carriers, the energy follows a stable trajectory around an equilibrium point which is characteristic of periodic oscillations (not shown).

The experiments were performed on the same cavity before and after a nitric acid surface treatment used to modify the carrier recombination time [25] and the quality factor. Nitric acid treatment introduces new surface states that modify the surface recombination velocity of the free-carriers and thus decrease the effective lifetime of the carriers. The silicon is also slightly etched by the nitric acid. The geometry of the PhC is thus modified and the Q factor is slightly increased. The experimental results are presented in Fig. 3(a) for a cavity with a quality factor of 90000 and various detunings. In Fig. 3(a), one observes self-induced oscillations with a period of 0.3 ns, for a laser wavelength detuned from -40 pm to -20 pm. The amplitude of the high-frequency oscillations is strongly damped with a characteristic decay time equal to $-\alpha_r^{-1} \approx 710$ ps and the oscillations at 3.18 GHz disappear before the end of the 10 -ns pulse. This characteristic time measured at a high input power corresponds to an increase of the photon lifetime in the cavity of one order of magnitude as compared to the photon lifetime $\tau = 75$ ps given by the Q factor at low power. This effective lifetime increase is a consequence of free-carrier induced nonlinearities that, in these experimental conditions, are not yet sufficient to generate self-sustained oscillations. Similar photon lifetime increases have been observed in active materials [26] using nonlinearities different from the one considered here.

The situation is strikingly different for the same cavity but this time with a Q factor of 130000 (i.e. after a nitric acid treatment) as shown in Fig. 3(b) for a detuning of -20 pm. Non-attenuated oscillations with a significant contrast are observed until the end of the pulse for a laser wavelength detuned from -30 pm to -10 pm. The oscillation frequency is 2.8 GHz, which is five times higher than the frequency of the oscillations observed in microring resonators (0.5 GHz) [16], notably because the quality factor of our cavity is about ten times lower than for the microring resonator, causing the cavity to react faster. This clearly demonstrates that self-sustained self-pulsing at GHz frequencies can be achieved in silicon photonic crystal nanocavities.

We have compared the experimental results with those obtained by the modeling described above. The only adjustable parameters were the free-carrier lifetime and the effective volume of the cavity. Only an effective volume close to $V_{eff} \simeq 5.25 \mu m^3$ could generate non-damped self-sustained oscillations with periods around 0.2 - 0.3 ns (see Fig. 2(a)). This value is in close

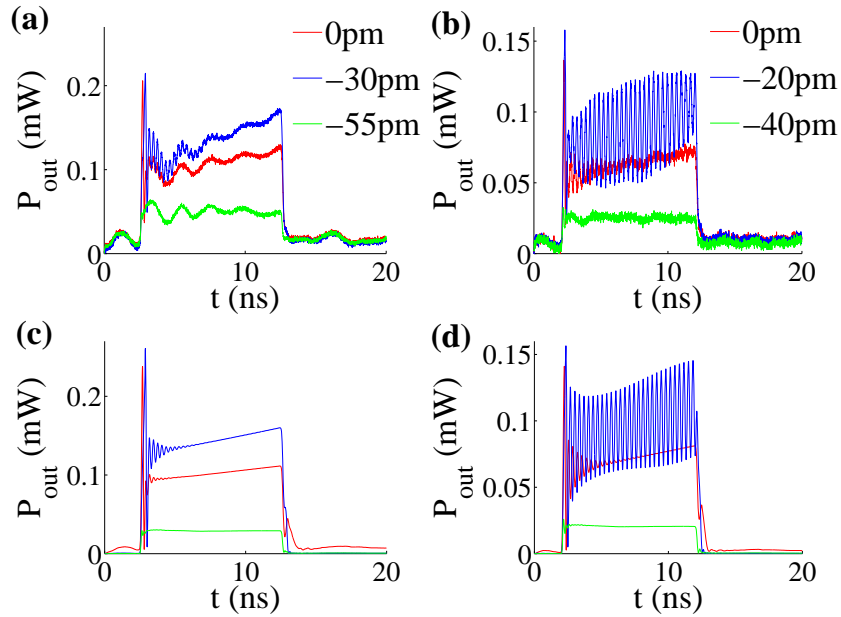


Fig. 3. Experimental (a and b) and simulated (c and d) output power as a function of time for different detunings between the laser wavelength and the resonance wavelength of the cavity. The input optical pulses have a length of 10 ns. Two types of cavities have been investigated. The first cavity has a quality factor of 9×10^4 and a resonance wavelength of 1590 nm. After the cavity had been immersed in a 3:1 $HNO_3:H_2O_2$ solution, the quality factor of the cavity increased, rising from 9×10^4 to 1.3×10^5 , and the resonance wavelength shifted to 1585.638 nm. Measurements (a) before and (b) after the nitric acid treatment. Corresponding modelings, (c) before nitric acid treatment ($Q=9 \times 10^4$ and $\tau_{fc} = 0.3$ ns) and (d) after the nitric acid treatment ($Q = 1.3 \times 10^5$ and $\tau_{fc} = 0.2$ ns). In Fig. 3(a), a parasitic extrinsic slow modulation of the signal is observed (period around 2 ns). This parasitic effect due to the measurement set-up was significantly suppressed for the subsequent measurements of the cavity [Fig. 3(b)].

agreement with a simple estimate that takes into account the diffusion length of the free-carriers in the slab (see appendix 1). A few values of the free-carrier lifetime were then tested to get the closest fits to the oscillation frequency. It was obtained for a free-carrier lifetime $\tau_{fc} = 0.3$ ns before the nitric acid surface treatment [Fig. 3(c)], and for a free-carrier lifetime $\tau_{fc} = 0.2$ ns after the nitric acid surface treatment [Fig. 3(d)]. Thermal dispersion is included in the equations (see appendix 4 thermal effects), to reproduce the increase of the output power with time as observed in the measurements but has no impact on the oscillation frequency.

If we consider that the transmitted signal is detected by a photodetector with a 1 A/W response and a 50 Ohm impedance circuitry, the radio-frequency power delivered by the nanocavity at 2.8 GHz is 20 nW. The radio-frequency power could also be collected directly by electrical contacts in close proximity of the photonic crystal thus eliminating the need for a fast photodetector [23]. These performances compare favorably with those achieved with spin-transfer nano-oscillators where a single spin-torque nano-oscillator emits a microwave power up to one nW [27]. Moreover, ultra-short free-carrier lifetime as small as 12 ps has been recently demonstrated in silicon nanowaveguides using a reverse bias and a p-i-n junction [28]. If we combine this lifetime value with a $Q=10000$ cavity, operation at 50 GHz can be expected for an input power of 50 mW with the advantage of generating the RF signal directly at the junction

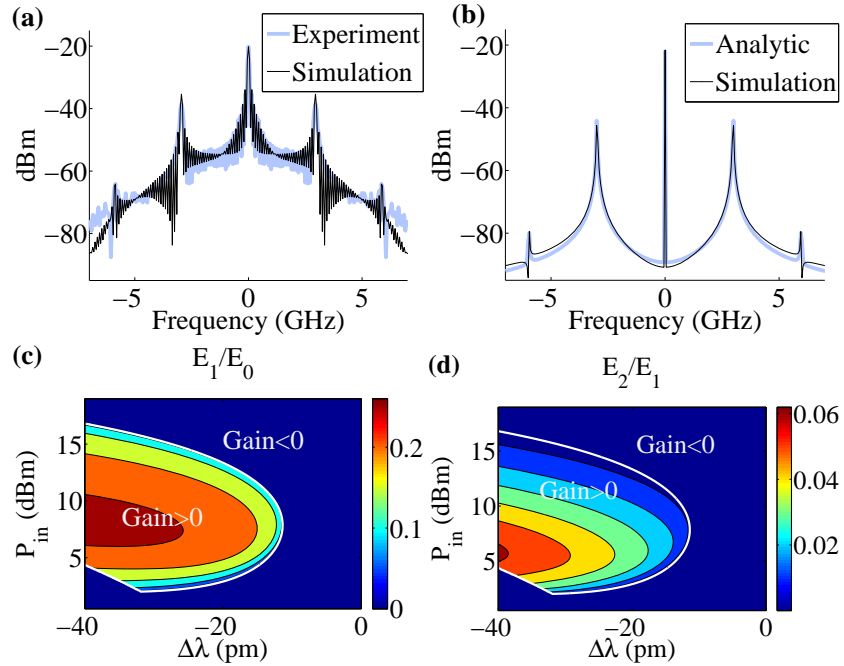


Fig. 4. : (a) Measured and simulated spectra of the oscillations with thermal effects for a detuning of -20 pm. (b) Comparison between the simulated and the analytically calculated spectra of the cavity with a continuous input power and without the thermal effects. (c) Ratio of the fundamental harmonic amplitude E_1 to the average energy in the cavity E_0 as a function of the input power and the detuning (analytical expression). (d) Ratio of the second harmonic amplitude E_2 to the fundamental amplitude E_1 (analytical expression).

electrical outputs. In III-V system, the same lifetime parameters lead to a 100 GHz operating frequency because of the difference of nonlinear coefficients [11]. As high-frequency operation requires low-Q cavities, self-pulsation could be easily observed with cavities on silicon-on-insulator with a further advantage of a better thermal management. Low-Q cavities can also exhibit lower cavity and effective volumes which are also an advantage for the onset of self-pulsing.

A remarkable property of the oscillations in PhC microcavity is their high spectral purity. As can be seen in Fig. 4(a), the amplitude of the second harmonic of $P_{Out} = |A|^2/\tau_{in}$, is 26 dB below the 2.8 GHz signal [29], as obtained after a Fourier transform of the measured and simulated signal. To explain this behavior, we solved Eqs. (1) and (2) in the harmonic regime (see appendix 5 solving the equations - harmonic analysis) where a solution for the stored energy in the cavity is approximated by $E \simeq E_0 + 2E_1 \cos(\Omega t + \varphi_1) + 2E_2 \cos(2\Omega t + \varphi_2)$. An excellent agreement is obtained between the analytical and simulated spectra [Fig. 4(b)] that confirms the validity of the method. From the analytical expressions of the energy in the cavity, we get the ratio of the second harmonic energy to the first one as: $E_2/E_1 = C_0 \times E_1/E_0$, where C_0 is a function of the frequency Ω , the average energy E_0 and the average number of free carriers. For oscillations triggered by an optical input power higher than 2 mW, the expressions of Ω , and C_0 , reduce to:

$$\Omega \sim \sqrt[5]{\frac{\tau_{fc} \gamma^{TPA} \gamma_i^{FCA}}{2(\hbar\omega)^2 V_{eff}}} \times T_{max} \left(\frac{P_{in}}{2\tau} \right)^2 - \frac{\Delta\omega}{5} \quad (3)$$

and

$$C_0 \sim \frac{1}{\Omega\tau_{fc}} \times \left(\left(1 + \frac{\Delta\omega}{\Omega} \right) - \frac{3\gamma^{TPA}\tau_{fc}E_0}{4\hbar\omega} \right) \quad (4)$$

where $\gamma_i^{FCA} = \text{Im}(\gamma^{FCA})$. These equations show that, counter intuitively, the signal is more sinusoidal at high injection power than at low power, because the frequency of the oscillations increases with the input power and C_0 decreases as the frequency increases. This behavior is confirmed in Fig. 4(c) and (d) that respectively represent E_1/E_0 and E_2/E_1 calculated with the complete analytical expression as a function of the input power and the detuning. Moreover, the amplitude of the harmonics is significantly smaller than the one observed in the microdisk resonator in [16], for which we have found that $E_2/E_1 = -14.6$ dB and $E_1/E_0 = -6$ dB, because the ratio E_1/E_0 and C_0 are higher in the microdisk, this last fact being explained by the higher frequency of the oscillations in the PhC microcavity. This higher oscillation frequency is a direct consequence of the smaller effective volume of the PhC cavity and of the lower quality factor which causes the system to react faster as seen in Eq. (3).

In conclusion, we have experimentally demonstrated that self-pulsing can occur at GHz frequencies in photonic crystal nanocavities. This self-pulsing effect differs significantly from the one created by thermal effects, which is limited to MHz frequencies. The operation frequency is here controlled by the carrier lifetime and photon lifetime in the cavity. Self-pulsing in photonic crystal cavities presents the advantage of simplicity to realize ultra-compact microwave sources with high spectral purity. As shown by the model we have developed, the remarkable spectral purity of the self-oscillations in PhC microcavities mainly results from the small volume of the PhC cavities and cannot be observed in larger cavities such as micro-disks. These microwave oscillators on an optical carrier are intrinsically compatible with optical delay lines based on dispersion engineering in photonic crystal waveguides, their combination allowing one the design of more complex architectures for microwave photonics.

Appendices:

1. Free-carrier dispersion, absorption and generation

The complex coefficient appearing in the third term of eq. (1), γ^{FCA} can be written as:

$$\gamma^{FCA} = \gamma_r^{FCA} + i\gamma_i^{FCA} = \frac{c}{2nR_{eff}} \left(\sigma_r - i\frac{2\omega}{c}\sigma_i \right) \times \left(\frac{\omega_r}{\omega} \right)^2 \quad (5)$$

The real and imaginary parts are responsible for absorption and dispersion respectively. $1/R_{eff}$ represents the fraction of the optical mode in the silicon part of the cavity calculated by a three-dimensional finite difference in time domain (FDTD) simulation ($R_{eff} = 1.1$). $\sigma_r = 1.45 \times 10^{-21} \text{ m}^2$ and $\sigma_i = -5.3 \times 10^{-27} \text{ m}^3$ are respectively the free-carrier absorption and dispersion in silicon given at $\lambda_r = 2\pi c/\omega_r = 1550 \text{ nm}$ [21].

The coefficient appearing in the fourth term of eq. (1), γ^{TPA} , can be expressed as [20]: $\gamma^{TPA} = (\beta\hbar\omega (\frac{c}{n})^2)/V_{TPA}$, where $\beta = 8.4 \times 10^{-12} \text{ m/W}$ [30] is the TPA coefficient in bulk silicon, $n = 3.48$ is the silicon refractive index [31], and $V_{TPA} = 4.8341 \times 10^{-19} \text{ m}^3$ is the TPA volume calculated by three-dimensional finite-difference in time domain modeling (FDTD).

2. Solving the equations: steady state and small perturbations

To solve the cavity equations, we wrote $A = |A|e^{i\varphi}$ and obtained two real equations from the first complex equation, which gave us a system of three real equations:

$$\frac{d|A|}{dt} = -\frac{|A|}{2\tau} - \gamma_r^{FCA}|A|\frac{N}{V_{eff}} - \frac{\gamma^{TPA}|A|^3}{2\hbar\omega} + \cos(\varphi)\sqrt{\frac{P_{in}}{\tau_{in}}} \quad (6)$$

$$\frac{d\varphi}{dt} = \Delta\omega - \gamma_i^{FCA} \frac{N}{V_{eff}} - \frac{\sin(\varphi)}{|A|} \sqrt{\frac{P_{in}}{\tau_{in}}} \quad (7)$$

$$\frac{dN}{dt} = -\frac{N}{\tau_{fc}} + \frac{1}{2} \gamma^{TPA} \frac{|A|^4}{(\hbar\omega)^2} \quad (8)$$

This system only differs from the one used in Ref. [11], in the fact that it is non-normalized and completely real. Looking for steady-state solutions ($|A_0|, \varphi_0, N_0$) to these equations, we get:

$$N_0 = \frac{\tau_{fc} \gamma^{TPA} |A_0|^4}{2(\hbar\omega)^2}, \quad (9)$$

$$\tan(\varphi_0) = \frac{\Delta\omega - \frac{\tau_{fc} \gamma^{TPA} \gamma_i^{FCA} |A_0|^4}{2(\hbar\omega)^2 V_{eff}}}{\frac{1}{2\tau} + \frac{\gamma^{TPA} |A_0|^2}{2\hbar\omega} + \frac{\tau_{fc} \gamma^{TPA} \gamma_i^{FCA} |A_0|^4}{2(\hbar\omega)^2 V_{eff}}}, \quad (10)$$

and $|A_0|^2$ is one of the roots of the five-degree polynomial:

$$\left(\frac{|A_0|}{2\tau} + \frac{\gamma^{TPA} |A_0|^3}{2\hbar\omega} + \frac{\tau_{fc} \gamma^{TPA} \gamma_i^{FCA} |A_0|^5}{2(\hbar\omega)^2 V_{eff}} \right)^2 + \left(\Delta\omega |A_0| - \frac{\tau_{fc} \gamma^{TPA} \gamma_i^{FCA} |A_0|^5}{2(\hbar\omega)^2 V_{eff}} \right)^2 - \frac{P_{in}}{\tau_{in}} = 0 \quad (11)$$

Linearizing these equations for small perturbations around these steady-state solutions gives:

$$\frac{d}{dt} \begin{pmatrix} \delta|A| \\ \delta\varphi \\ \delta N \end{pmatrix} = M \begin{pmatrix} \delta|A| \\ \delta\varphi \\ \delta N \end{pmatrix}, \quad (12)$$

$$M = \begin{pmatrix} -\frac{1}{2\tau} - \frac{\gamma_i^{FCA} N_0}{V_{eff}} - \frac{3\gamma^{TPA} |A_0|^2}{2\hbar\omega} & -\sin(\varphi_0) \sqrt{\frac{P_{in}}{\tau_{in}}} & -\frac{\gamma_i^{FCA} |A_0|}{V_{eff}} \\ \frac{\sin(\varphi_0)}{|A_0|^2} \sqrt{\frac{P_{in}}{\tau_{in}}} & -\frac{\cos(\varphi_0)}{|A_0|} \sqrt{\frac{P_{in}}{\tau_{in}}} & -\frac{\gamma_i^{FCA}}{V_{eff}} \\ \frac{2\gamma^{TPA} |A_0|^3}{(\hbar\omega)^2} & 0 & -\frac{1}{\tau_{fc}} \end{pmatrix} \quad (13)$$

The eigenvalues of this matrix can be calculated as a function of $|A|$ only and determine the linearized system behaviour. Self-induced oscillations are possible when the matrix M is characterized by a Hopf bifurcation, which happens when M has a pair of complex conjugate eigenvalues $\alpha_r \pm i\Omega$ which crosses the imaginary axis into the right half complex plane, i.e. the real part of the eigenvalue becomes positive as a parameter of the system is varied. These oscillations are non-attenuated for $\alpha_r > 0$, and their period is $T = 2\pi/\Omega$.

In Eq. (11), for input power in the range considered here, typically $P_{in} > 2$ mW in the case of the PhC cavity, from Eq. (11), we have $\frac{\tau_{fc} \gamma^{TPA} \gamma_i^{FCA} |A_0|^5}{2(\hbar\omega)^2 V_{eff}} \sim \sqrt{\frac{P_{in}}{\tau_{in}}} + \Delta\omega |A_0|$ because $\gamma_i^{FCA} \gg \gamma_r^{FCA}$. Note that the detuning $\Delta\omega$ cannot be neglected since it has still a significant influence on the energy inside the cavity as can be seen on Fig. 1(b). One then gets the approximate expression:

$$|A_0| \sim \sqrt[5]{\frac{2(\hbar\omega)^2 V_{eff}}{\tau_{fc} \gamma^{TPA} \gamma_i^{FCA}} \left(\frac{P_{in}}{\tau_{in}} \right)^{1/2}} \times \left(1 - \frac{\Delta\omega}{5} \times \sqrt[5]{\frac{2(\hbar\omega)^2 V_{eff}}{\tau_{fc} \gamma^{TPA} \gamma_i^{FCA}} \left(\frac{\tau_{in}}{P_{in}} \right)^2} \right)^{-1} \quad (14)$$

. Neglecting small terms in the matrix M , we have $\Omega |A_0| \approx \sqrt{P_{in}/\tau_{in}}$ and

$$\Omega \sim \sqrt[5]{\frac{\tau_{fc} \gamma^{TPA} \gamma_i^{FCA}}{2(\hbar\omega)^2 V_{eff}}} \times T_{max} \left(\frac{P_{in}}{2\tau} \right)^2 - \frac{\Delta\omega}{5}. \quad (15)$$

3. Estimating the cavity effective volume

The cavity effective volume for the free-carriers found experimentally ($V_{eff} \simeq 5.25 \mu\text{m}^3$) is ten times larger than the cavity volume used in Ref. [20], where it is calculated as $V_{eff} = (2d) \times (\sqrt{3}a) \times h$, with $d \simeq 1.1 \mu\text{m}$ the diffusion length of the free-carriers, h the slab thickness, and $\sqrt{3}a$ the distance between the air holes nearest to the center of the cavity in the orthogonal direction (a being the photonic crystal period). Using this formula would give $V_{eff} = 0.32 \mu\text{m}^3$ for the investigated cavity. But this model assumes that the free-carrier diffusion stops at the air holes, which is not the case. According to Ref. [32], the diffusion of free-carriers in a photonic crystal is not very different from the diffusion of free-carriers in a silicon membrane without holes. Furthermore, it assumes that the free-carriers are all created in the cavity center, but the electric field profile of the cavity resonant mode calculated by FDTD is in fact quite large and is included in a volume approximately equal to $(8a) \times (2\sqrt{3}a) \times h$. If we assume that the free-carriers are created uniformly in this volume, and then diffuse in the rest of the cavity, we can approximate the effective cavity volume for the free-carriers by $V_{eff} = (8a + 2d) \times (2\sqrt{3}a + 2d) \times h$. This formula gives $V_{eff} = 4.06 \mu\text{m}^3$, which is close to the value of V_{eff} that was deduced from the experimental measurements.

4. Thermal effects

If we take into account the thermal dispersion, the equations used for the modeling become [14]:

$$\frac{dA}{dt} = -\frac{A}{2\tau} + i\Delta\omega A - \gamma^{FCA} A \frac{N}{V_{eff}} - i\gamma^T A \Delta T - \frac{\gamma^{TPA} |A|^2 A}{2\hbar\omega} + \sqrt{\frac{P_{in}}{\tau_{in}}} \quad (16)$$

$$\frac{dN}{dt} = -\frac{N}{\tau_{fc}} + \frac{1}{2} \gamma^{TPA} \frac{|A|^4}{(\hbar\omega)^2} \quad (17)$$

$$(\rho_{Si} C_p^{Si} V_{eff}^T) \frac{d\Delta T}{dt} = -\frac{\Delta T}{R_T} + \hbar\omega (\gamma^{TPA} \frac{|A|^4}{(\hbar\omega)^2} + 2\gamma_r^{FCA} \frac{|A|^2}{\hbar\omega} \frac{N}{V_{eff}}) \quad (18)$$

where ΔT is the temperature difference in the cavity generated by the input power, $\rho_{Si} = 2.33 \text{ g/cm}^3$ is the silicon density, $C_p^{Si} = 0.7 \text{ J/(g}\times\text{K)}$ is the thermal capacity of silicon, and $\gamma^T = -\frac{\omega}{n} \frac{dn}{dT}$ is the thermal dispersion with $\frac{dn}{dT} = 1.86 \times 10^{-4} \text{ K}^{-1}$ [14]. Two parameters are unknown: the thermal resistance of the cavity R_T and the effective cavity volume that depends on the temperature V_{eff}^T . To determine these two coefficients, measurements on the cavity after nitric acid treatment were performed again with pulses of 200 ns length. These measurements allowed us to observe thermal oscillations with a frequency around 20 MHz. We used these oscillations to determine approximate values of the thermal resistance and effective volume by comparing measurements and modeling, and found $R_T \approx 8 \times 10^3 \text{ K/W}$ and $V_{eff}^T \approx 3 \times 10^{-18} \text{ m}^3$, which were used in the modeling as shown in Fig. 3(c) and 3(d).

5. Solving the equations: harmonic analysis

An approximate analytical expression for the time evolution $E(t) = |A(t)|^2$ of the energy in the cavity can be obtained when the harmonic regime is reached for a constant input power. The sketch of the method is the following. First, in Eq. (2), we neglected higher order harmonics of $|A|^2$, the stored energy in the cavity, and replaced it by the approximation $|A|^2 \simeq A_0^{(2)} + 2A_1^{(2)} \cos(\Omega t + \varphi_{A_1^{(2)}})$ with $\varphi_{A_1^{(2)}}$ a phase term introduced for generality. We then solved the linear first order differential equation that is obtained for N , the number of free carriers. This expression for N and the approximate value of $|A|^2$ are used to transform Eq. (1) in a first order,

linear, ordinary differential equation of the form: $dA/dt \simeq -(R + F(t))A + \sqrt{P_{in}/\tau_{in}}$ where R is a constant and $F(t)$ is a sum of two sinusoids. Solving this equation and taking the square modulus of its solution, we get for the energy, $E \simeq E_0 + 2E_1 \cos(\Omega t + \varphi_1) + 2E_2 \cos(2\Omega t + \varphi_2)$ where E_0, E_1, E_2 depend on $A_0^{(2)}$ and $A_1^{(2)}$. For consistency, this expression of E must be equal to the first approximation we initially used in Eqs. (1) and (2), i.e. $E_0 = A_0^{(2)}, E_1 = A_1^{(2)}$ with E_2 negligible. Finally, solving these last two equations gives expressions for E_0, E_1 and E_2 .

The detailed calculation is given in the following. According to the experimental results, if we neglect thermal effects, the time evolution of the energy is quasi-sinusoidal. The energy can then be written as:

$$|A(t)|^2 \simeq A_0^{(2)} + 2A_1^{(2)} \cos(\Omega t + \varphi_{A_1^{(2)}}) \quad (19)$$

and $|A|^4 = E(t)^2 \simeq ((A_0^{(2)})^2 + 2(A_1^{(2)})^2) + 4A_0^{(2)}A_1^{(2)} \cos(\Omega t + \varphi_{A_1^{(2)}})$ plus an harmonic term that is neglected. Equation (2) becomes :

$$\frac{dN}{dt} \simeq -\frac{N}{\tau_{fc}} + \frac{1}{2} \frac{\gamma^{TPA}}{(\hbar\omega)^2} [(A_0^{(2)})^2 + 2(A_1^{(2)})^2 + 4A_0^{(2)}A_1^{(2)} \cos(\Omega t + \varphi_{A_1^{(2)}})] \quad (20)$$

Solving this linear first order differential equation, we get the following expression for N : $N(t) = N_0 + 2N_1 \cos(\Omega t + \varphi_{N1})$, with $N_0 = \frac{\tau_{fc}\gamma^{TPA}((A_0^{(2)})^2 + 2(A_1^{(2)})^2)}{2(\hbar\omega)^2} \simeq \frac{\tau_{fc}\gamma^{TPA}(A_0^{(2)})^2}{2(\hbar\omega)^2}$, $N_1 = \frac{\tau_{fc}\gamma^{TPA}2A_0^{(2)}A_1^{(2)}}{2(\hbar\omega)^2(1+i\Omega\tau_{fc})}$ and φ_{N1} a phase term. Replacing this expression of N in the Eq. (1), we get the first order, linear, ordinary differential equation :

$$\frac{dA}{dt} \simeq -(R + F(t))A + \sqrt{\frac{P_{in}}{\tau_{in}}} \quad (21)$$

with

$$R = \frac{1}{2\tau} - i\Delta\omega + \frac{\gamma^{FCA}N_0}{V_{eff}} + \frac{\gamma^{TPA}A_0^{(2)}}{2\hbar\omega} \quad (22)$$

$$F(t) = \frac{2\gamma^{FCA}N_1}{V_{eff}} \cos(\Omega t + \varphi_{N1}) + \frac{2\gamma^{TPA}A_1^{(2)}}{2\hbar\omega} \cos(\Omega t + \varphi_{A_1^{(2)}}) \quad (23)$$

For time $t \gg 1/R$, the harmonic regime is reached and the solution of this equation is :

$$A(t) = Ke^{-Rt - \int_0^t F(t')dt'} \int_0^t e^{Rt' + \int_0^{t'} F(t'')dt''} dt' \quad (24)$$

with $\int_0^t F(t')dt' = \alpha_1^{FCA} \sin(\Omega t + \varphi_{N1}) + \alpha^{TPA} \sin(\Omega t + \varphi_{A_1^{(2)}})$, $K = \sqrt{\frac{P_{in}}{\tau_{in}}}$, $\alpha^{TPA} = \frac{2}{\Omega} \frac{\gamma^{TPA}A_1^{(2)}}{2\hbar\omega}$ and $\alpha^{FCA} = \frac{2}{\Omega} \frac{\gamma^{FCA}N_1}{V_{eff}}$.

In the case of a photonic crystal cavity with an input power of 2 mW and a detuning of -20 pm, as in the experiments, we have $\alpha^{TPA} = 0.016$ and $\alpha^{FCA} = 0.004 + 0.123i$ and the main contribution to the integral $\int_0^t F(t')dt'$ comes from the imaginary part of α^{FCA} . To further simplify the calculations, we, first, only consider this contribution in the evaluation of R and of the integral $\int_0^t F(t')dt'$, i.e. $R \approx \frac{1}{2\tau} + i(\frac{\gamma^{FCA}N_0}{V_{eff}} - \Delta\omega)$ and $\int_0^t F(t')dt' \approx \alpha_i^{FCA} \sin(\theta)$ with $\alpha_i^{FCA} = \frac{2}{\Omega} \frac{\gamma_i^{FCA}N_1}{V_{eff}}$, $\gamma_i^{FCA} = \text{Im}(\gamma^{FCA})$ and $\theta = \Omega t + \varphi_{N1}$.

The Jacobi-Anger expansion is used to develop $e^{jF(t)}$ as :

$$e^{j\int_0^t F(t')dt'} \approx e^{\alpha_i^{FCA} \sin(\theta)} = \sum i^{3n} I_n(\alpha_i^{FCA}) e^{in\theta} \quad (25)$$

where the I_n are the modified Bessel functions of the first kind. In this expansion, only the terms for $n = -1, 0$ and 1 are conserved as it can be checked that the influence of other terms on the final values of the fundamental and the second harmonic is negligible as compared to the influence of $I_1(\alpha_i^{FCA})(e^{i\theta} - e^{-i\theta})$ in the case of our experimental conditions. As a consequence, we have the following expressions :

$$\int_0^t e^{Rt' + j\int_0^{t'} F(t'')dt''} dt' = e^{Rt} \left[\frac{I_0(\alpha_i^{FCA})}{R} - iI_1(\alpha_i^{FCA}) \left(\frac{e^{i\theta}}{R+i\Omega} - \frac{e^{-i\theta}}{R-i\Omega} \right) \right] \quad (26)$$

and

$$A = K \left(\frac{I_0(\alpha_i^{FCA})}{R} - iI_1(\alpha_i^{FCA}) \left(\frac{e^{i\theta}}{R+i\Omega} - \frac{e^{-i\theta}}{R-i\Omega} \right) \right) e^{-\alpha_i^{FCA} \sin(\theta)} \quad (27)$$

We then deduced the energy as:

$$E = |A|^2 = K^2 \left| \frac{I_0(\alpha_i^{FCA})}{R} - iI_1(\alpha_i^{FCA}) \left(\frac{e^{i\theta}}{R+i\Omega} - \frac{e^{-i\theta}}{R-i\Omega} \right) \right|^2 \quad (28)$$

that can be decomposed as

$$E = (E_0 + 2E_1 \cos(\Omega t + \varphi_1) + 2E_2 \cos(2\Omega t + \varphi_2)) \quad (29)$$

with

$$E_0 = K^2 \left(\frac{I_0(\alpha_i^{FCA})^2}{|R|^2} + \frac{2|I_1(\alpha_i^{FCA})|^2(\Omega^2 + |R|^2)}{(|R|^2 - \Omega^2)^2 + (2\Omega \text{Re}(R))^2} \right) \quad (30)$$

$$E_1 = K^2 \frac{2\Omega \text{Im}(R) I_0(\alpha_i^{FCA}) |I_1(\alpha_i^{FCA})|}{\sqrt{(|R|^2 - \Omega^2)^2 + (2\Omega \text{Re}(R))^2}} \quad (31)$$

and

$$E_2 = K^2 \frac{|I_1(\alpha_i^{FCA})|^2}{\sqrt{(|R|^2 - \Omega^2)^2 + (2\Omega \text{Re}(R))^2}} \quad (32)$$

For consistency, this expression of E must be equal the one initially introduced in Eq. (19), i.e. $E_0 = A_0^{(2)}$, $E_1 = A_1^{(2)}$ with E_2 negligible. We then get a set of two transcendental equations, the first one in the unknown $A_0^{(2)}$ and the second one in the unknown $A_0^{(2)}$ and $A_1^{(2)}$, $A_1^{(2)}$ being one of the harmonic magnitudes we are looking for. The magnitude of the fundamental $A_1^{(2)}$ can be determined by solving numerically the equation $A_1^{(2)} = E_1$ and the amplitude of the second harmonic can then be calculated by using the expression of E_2 . A simple expression can be obtained for the ratio of the second harmonic to the first one E_2/E_1 :

$$\frac{E_2}{E_1} \simeq \frac{|I_1(\alpha_i^{FCA})|^2}{2\Omega \text{Im}(R) I_0(\alpha_i^{FCA}) |I_1(\alpha_i^{FCA})|} \quad (33)$$

In the conditions of the experiment, $|\alpha_i^{FCA}| \ll 1$, $I_0(\alpha_i^{FCA}) \sim 1$, $I_1(\alpha_i^{FCA}) \sim \frac{1}{2} \alpha_i^{FCA} = \frac{i\gamma_i^{FCA} N_1}{\Omega V_{eff}}$, and we get:

$$\frac{E_2}{E_1} \simeq C_0 \times \frac{E_1}{E_0} \quad (34)$$

where

$$C_0 = \frac{\gamma_i^{FCA} N_0}{V_{eff}} \frac{|R|^2}{\Omega^2 \text{Im}(R) \sqrt{1 + \Omega^2 \tau_{fc}^2}} \quad (35)$$

C_0 depends only on N_0 and Ω , which are easily calculated from the steady-state solutions and the eigenvalues of the linearized system (see above: solving the equations: steady state and small perturbations).

For oscillations triggered by an input optical power higher than 2 mW, the expressions of Ω and R reduce to $\Omega \sim \frac{\gamma_i^{FCA} N_0}{V_{eff}} - \Delta\omega$ and $R \sim i\Omega$, and the expression of C_0 simplify to

$$C_0 \sim \frac{\gamma_i^{FCA} N_0}{\tau_{fc} \Omega^2 V_{eff}} \sim \frac{1}{\Omega \tau_{fc}} \times \left(1 + \frac{\Delta\omega}{\Omega} \right) \quad (36)$$

C_0 will be lower at high frequencies, i.e. the signal will be more sinusoidal.

The same method can be used if the two-photon absorption and the free carrier absorption are taken into account in the calculation of Eq. (24). The expressions of E_0 , E_1 , E_2 and C_0 then become more complicated but they still simplify for an input optical power higher than 2 mW and we get for C_0 :

$$C_0 \sim \frac{1}{\Omega \tau_{fc}} \times \left(\left(1 + \frac{\Delta\omega}{\Omega} \right) - \frac{3\gamma^{TPA} \tau_{fc} E_0}{4\hbar\omega} \right) \quad (37)$$

Numerically, for a detuning of -20 pm, C_0 varies between 0.27 and 0.084 for an input power varying from 1.5 mW to 20 mW. For $P_{in} = 2$ mW, $C_0 = 0.24$ and $E_1/E_0 = -21.4$ dB, which gives us $E_2/E_1 \simeq -33.6$ dB, which is very close to the values found by the numerical simulation (see Fig. 4b) : $E_1/E_0 = -21.3$ dB and $E_2/E_1 = -34.7$ dB. The amplitude of the second harmonic is very low compared to the fundamental, which justifies the approximation of the energy function by a sinusoid we made at the beginning.

In the case of a microring resonator of the kind described in Ref. [16], we have according to our simulations $\alpha^{TPA} = 0.042$ and $\alpha^{FCA} = 0.04 + 1.21i$ for a detuning of -2.5 pm and an input power of 1 mW. Since $|\alpha^{FCA}| > 1$, we can no longer write $e^{\alpha_i^{FCA} \sin(\theta)} \sim I_0(\alpha_i^{FCA}) - iI_1(\alpha_i^{FCA})(e^{i\theta} - e^{-i\theta})$, $I_0(\alpha_i^{FCA}) \sim 1$ nor $I_1(\alpha_i^{FCA}) \sim \frac{1}{2}\alpha_i^{FCA}$, and the formulae above are no longer very accurate. However, they can still be used to estimate the importance of the second harmonic. Numerically, for a detuning of -2.5 pm and an input power $P_{in} = 1$ mW, similar to the experimental parameters used in Ref. [16], $C_0 = 0.37$, $E_1/E_0 = -6$ dB and $E_2/E_1 \simeq -14.6$ dB according to the formula (37), a value which is close to the value given by a full numerical simulation (- 15 dB). Therefore, we can conclude that the greater nonlinearity of the oscillations in a microring resonator is caused firstly by the higher value of C_0 , itself explained by the lower value of the frequency of the oscillations in a microdisk, and secondly by the higher amplitude of those oscillations.

Acknowledgments

This work was supported by the Agence Nationale de la Recherche (ANR) through the project PHLORA (ANR 2010 JCJC 0304 01). This work was also supported by the french RENATECH network and Conseil général de l'Essonne.